

Global MHD Stability Study of KSTAR High Beta Plasma Equilibria Under Passive and Active Mode Control

O. Katsuro-Hopkins 1), S.A. Sabbagh 1), J.M. Bialek 1), H.K. Park 2), J. G. Bak 3), J. Chung 3), S.H. Hahn 3), J.Y. Kim 3), M. Kwon 3), S.G. Lee 3), S.W. Yoon 3), K.-I. You 3), A.H. Glasser 4), L.L. Lao 5)

1) Department of Applied Physics and Applied Mathematics, Columbia University, New York, NY, USA

2) Pohang University of Science and Technology, Pohang, Korea

3) National Fusion Research Institute, Daejeon, Korea

4) Los Alamos National Laboratory, Los Alamos, NM, USA

5) General Atomics, San Diego, CA, USA

email contact of the main author: onk@pppl.gov

Abstract. The Korea Superconducting Tokamak Advanced Research, KSTAR, is designed to operate a steady-state, high beta plasma while retaining global magnetohydrodynamic (MHD) stability to establish the scientific and technological basis of an economically attractive fusion reactor. Global MHD mode stabilization can be achieved by equilibrium profile optimization, passive control via plasma rotation, and active control. Evaluating and verifying advanced MHD control systems gives greater confidence for stabilization of future devices, including the advanced scenario operation of ITER. An EFIT equilibrium model is established for stability analysis of KSTAR. Reconstructions were performed for the experimental start-up scenario and first plasmas. The VALEN 3D code was used to determine the vacuum vessel current distribution for vacuum field start up. Theoretical high beta equilibria spanning the expected operational range are computed for various profiles including generic L-mode and DIII-D experimental H-mode pressure profiles. Ideal MHD stability calculations of toroidal mode number of unity using DCON shows a factor of two improvement in the plasma beta limit over the no-wall beta limit at moderate to low plasma internal inductance. The planned stabilization system in KSTAR comprises passive stabilizing plates and actively cooled in-vessel control coils (IVCC) designed for non-axisymmetric field error correction and stabilization of slow timescale MHD modes including resistive wall modes (RWM). VALEN analysis using standard proportional gain shows that active stabilization near the ideal wall limit was reached with feedback gain 1.0 – 10V/G using the midplane segment of the IVCC. For a fast IVCC coil circuit with $L/R = 1.0\text{ms}$ the upper limit of the RMS power required for control using noise taken from NSTX active stabilization experiments is computed to be on the order of 1MW for beta near the ideal wall limit. Advanced state-space control algorithms yield a factor of 2 power reduction assuming white noise while remaining robust with respect to variations in plasma beta.

1. Introduction

The efficiency of tokamak fusion reactors is improved by operating at the highest possible values of toroidal and normalized plasma beta $\beta_t \equiv 2\mu_0 \langle p \rangle / B_0^2$ and $\beta_N \equiv 10^8 \langle \beta_t \rangle a B_0 / I_p$, while minimizing re-circulated power required to drive the plasma current. Here p is the plasma pressure, B_0 is the vacuum toroidal field at the plasma geometric center, a is the plasma minor radius at the midplane, I_p is the plasma current, and brackets represent volume average. In addition, maximizing the bootstrap current [1] minimizes the amount of external current drive power required to maintain steady-state plasma operation. Such operation typically leads to relatively broad current profiles and therefore reduced plasma internal inductance, l_i . Fortunately, such equilibria are typically amenable to stabilization of global magnetohydrodynamic (MHD) modes that limit beta. Fusion power scales as β_i^2 and at constant levels of bootstrap current (constant poloidal beta) scales as β_N^4 , so even a modest increase in β_N can be significant [2]. Favorable experimental performance has been demonstrated in advanced operating regimes of present tokamaks with increased β_N in which

conventional ideal MHD no-wall stability limits are exceeded by either passive [3] [4] and/or active [5] [6] [7] means.

The Korea Superconducting Tokamak Advanced Research (KSTAR) [8] [9] device is an advanced superconducting tokamak designed to operate a steady-state, high β_N plasma stabilized by passive or active means to establish the scientific and technological basis of an attractive fusion reactor. KSTAR has major radius, $R_0 = 1.8\text{m}$, minor radius, $a = 0.5\text{m}$, toroidal field, $B_{t0} = 3.5\text{T}$, and plasma current, $I_p = 2\text{MA}$, with a strongly shaped plasma cross-section, double null divertor, and is designed for pulse lengths up to 300s. The KSTAR device has been constructed and first plasma operation was successfully accomplished in June, 2008. During the first experiments KSTAR has achieved a maximum $I_p = 130\text{kA}$ and pulse length exceeding 0.8 s at toroidal magnetic field $B_t = 1.5\text{T}$.

In the present paper, we compute KSTAR first plasma reconstructions and further the work of the original physics design of the machine [10] by theoretically examining the high β operating space accessible when stabilizing kink/ballooning modes and resistive wall modes (RWM). With mode stabilization, β_N can be significantly increased in KSTAR to values exceeding 5, thereby doubling the computed ideal MHD no-wall β_N limit, $\beta_{N(n=1)}^{no-wall}$. Here, n is the toroidal mode number. In this paper, $\beta_N^{no-wall} \equiv \beta_{N(n=1)}^{no-wall}$. Section 2 shows first plasma equilibrium reconstruction and the technique used to produce it. Section 3 describes achievable equilibria for L-mode and H-mode pressure profiles, illustrating the equilibrium operating space by the variables (I_i, β_N) and ideal MHD stability for kink/ballooning modes with $n = 1 - 2$ both with and without passive stabilizing structure. Section 4 examines $n = 1$ RWM growth rates, showing the capability of the IVCC coil for RWM stabilization. Section 5 investigates advanced control methods for RWM stabilization resulting in a factor of 2 power reduction assuming white noise. Section 6 summarizes the results and considers implications for future stabilization experiments based on recent experimental experience and comparison to the present analysis.

2. Equilibrium reconstruction

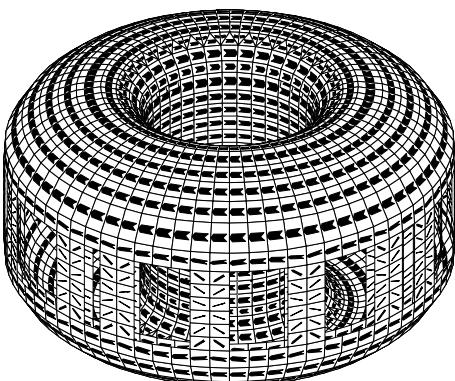


FIG. 1. Currents in the VALEN double-walled vacuum vessel of KSTAR

In preparation for first plasma experiments, equilibria were produced in EFIT [11] using the planned experimental start-up scenario including transient vacuum vessel currents as computed by the VALEN code [12]. The techniques, specific additions, and constraints required to model the KSTAR configuration are similar to those used in NSTX equilibrium reconstruction, as summarized in Ref. [13]. Details specific to KSTAR equilibrium reconstruction are described in this section.

The 3D VALEN model of the KSTAR double-walled vacuum vessel with port penetrations at the actual locations (Fig.1) was used to model the time evolution of vessel currents for the reference startup scenario with field null at low $R \sim 1.6\text{m}$. The time trace of ohmic, shaping, and radial force balance (PF) coil currents and calculated total vacuum vessel current are shown in Fig.2. There is good agreement between 2D modeling and 3D VALEN modeling with the total wall current peak value of -128kA reached at time 0.04 s.

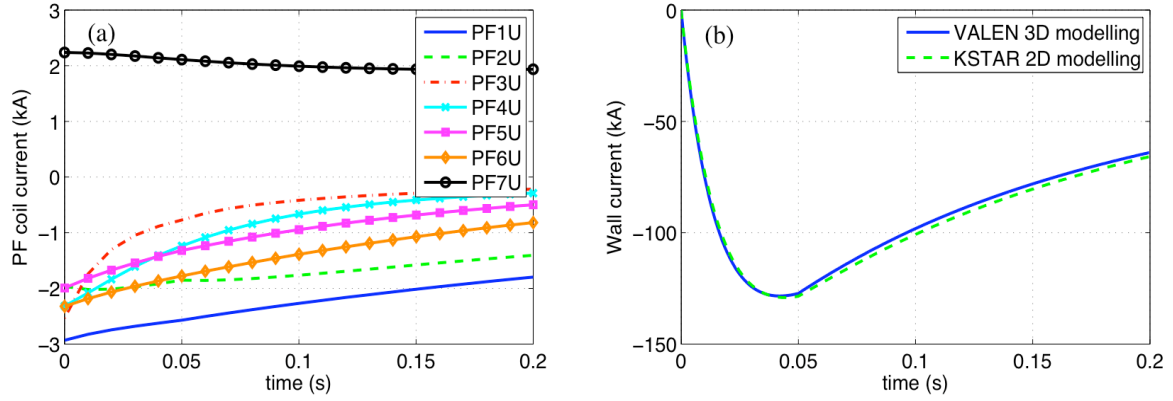


FIG. 2. (a) Start up scenario 1 PF coil current evolution and (b) total wall current: 3D VALEN modeling compared with 2D modeling.

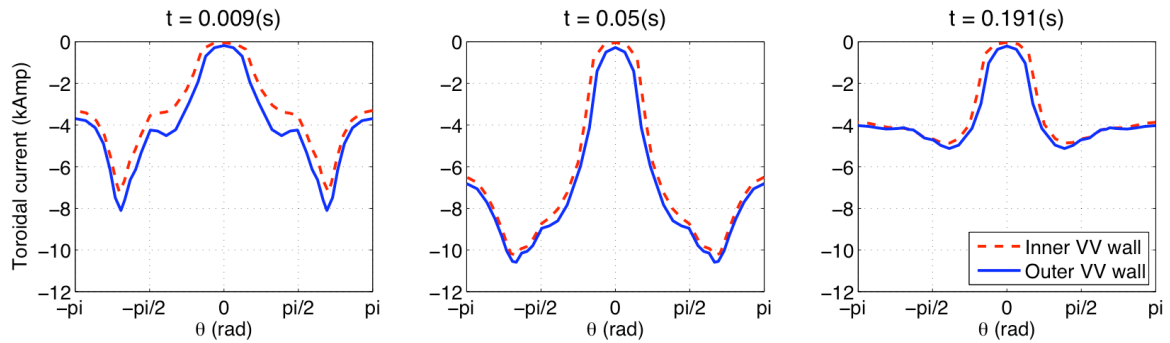


FIG. 3. Poloidal distribution of toroidal current on inner and outer vacuum vessel (VV) walls for various times during scenario 1 start up.

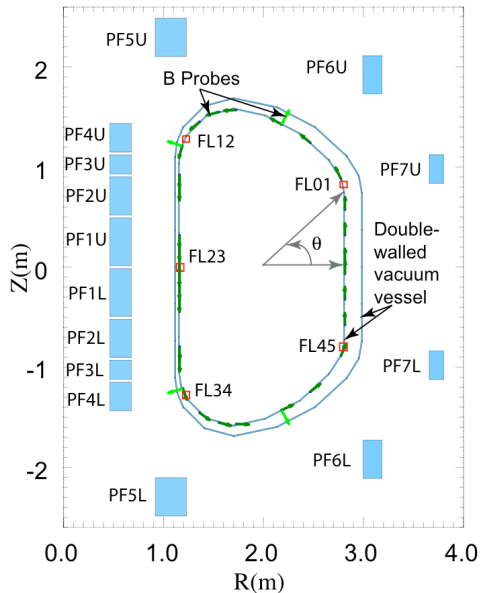


FIG. 4. KSTAR configuration used in EFIT calculations.

the device, illustrating conducting structure, location of the PF coils and flux-loops, is shown in Fig. 4. Magnetic probes distributed poloidally over the inside of vacuum vessel are also shown. The vacuum vessel is modeled as a collection of single turn parallel conductors. Inner and outer vessels are each divided into 28 independent current carrying regions. An effective resistance for each region is determined from VALEN calculations by using the most constant

The time evolution of the poloidal distribution of toroidal current in the inner and outer vacuum vessel walls, needed for first plasma equilibrium reconstruction is shown in Fig.3 for three time points – shortly after the flux swing, at the time of peak current and later in the evolution of scenario 1. Near-zero current corresponds to the port penetration region, ($\theta = 0$) and the maximum values occur at the upper and lower vacuum vessel segments at the lowest major radius, which are lowest resistance path around the torus ($\theta \cong \pm 125^\circ$).

Initial KSTAR equilibrium reconstructions utilize data from 14 PF coil currents, 5 flux loop voltages, 28 magnetic probes, a Rogowski coil measuring the total toroidal plasma current, and estimated vacuum vessel currents based on VALEN vacuum field modeling [14]. The poloidal cross-section of

ratio over the simulation time period of the voltage measured in a loop voltage sensor neighboring the toroidal current in that region, yielding effective resistance, $R_{eff;i} = V_{loop;i}/I_i$, as shown in Fig. 5.

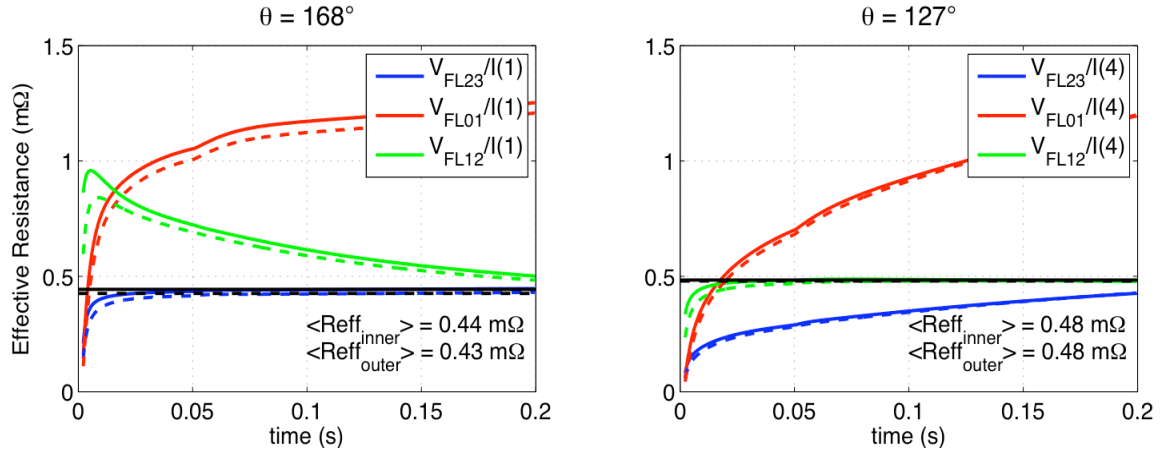


FIG. 5. Effective resistance for inner (solid line) and outer (dashed line) vacuum vessel walls at different poloidal location θ of the wall elements. For the vessel segment at $\theta=168^\circ$ voltage from flux loop FL23 is used in reconstructions, at $\theta=127^\circ$ FL12 is used.

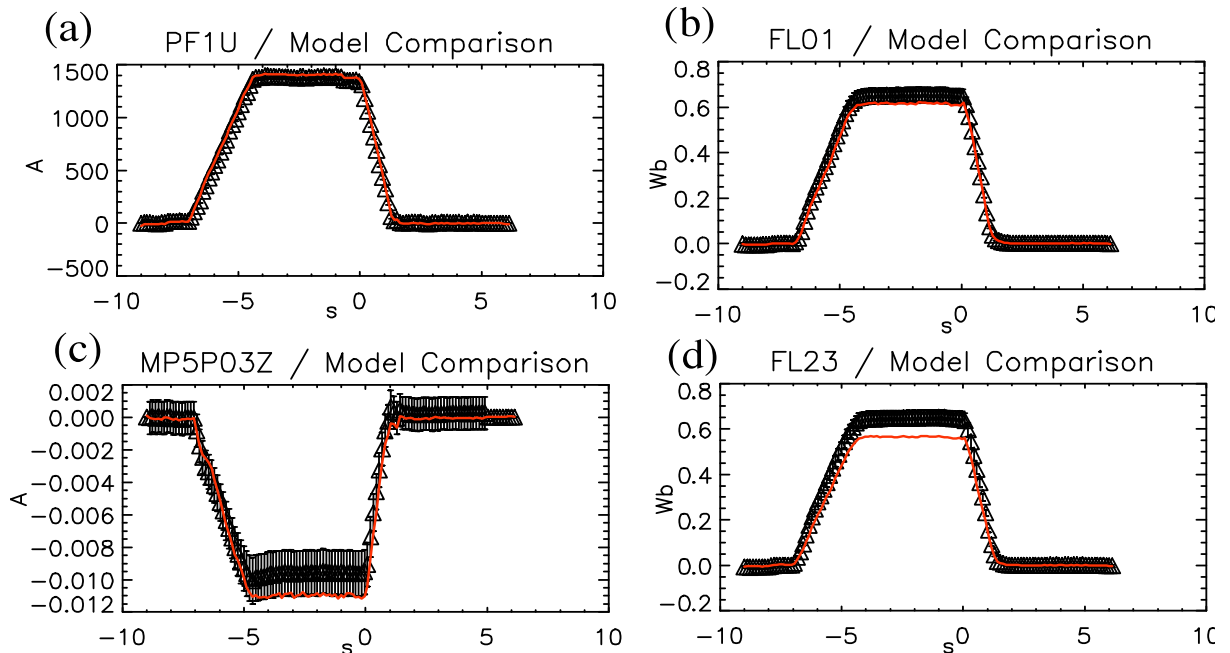


FIG. 6. Examples of EFIT vacuum field reconstruction for combined vacuum fields shot 964. Model and experimental data comparison PF1U coil (a); outboard midplane magnetic probe signal magnetic probe signal MP5P01Z (c) and Flux loop FL01(b) and FL23 (d)

The reconstruction of several measured currents, flux loops and magnetic signals is illustrated in Fig. 6 for combined vacuum field shot 964. Each time point corresponds to a single reconstruction. Fig. 6 shows a good match of the modeled and measured PF1U coil current. Flux loop FL01 on the outboard side, shown in the top right corner of Fig.6, has better agreement than flux loop FL23, inboard side, shown in the bottom right corner of Fig. 6. This may be due to the presence of paramagnetic Incoloy material used in some of the poloidal and toroidal field coils. Effects of Incoloy were not accounted in the initial EFIT analysis. Measured and modeled data for magnetic probe MP5P01Z is given in the bottom left corner of Fig. 6. For initial analysis, magnetic probes were given the largest relative errors between

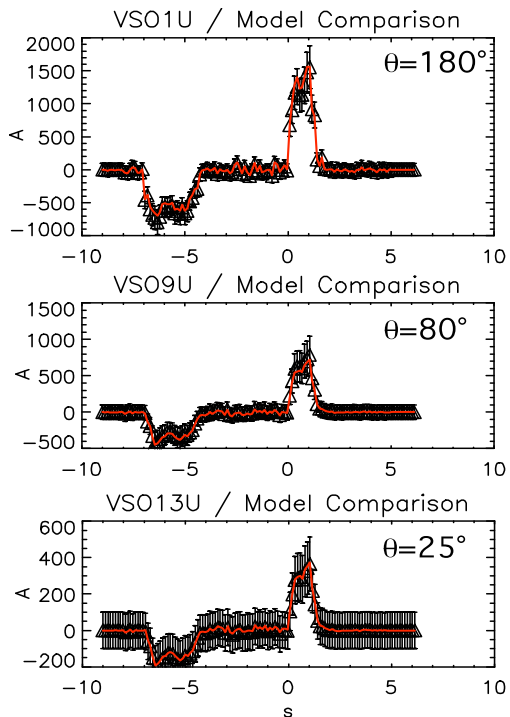


FIG. 7. Vacuum field reconstruction with EFIT, vessel segments, shot 964.

5-10%. Results typically match within the error with total χ^2 ranging from <100 to ~ 500 (χ^2 ranges from 40 to 115 for shot 962). Fig. 7 illustrates a representative subset of the vessel segments currents. A large relative error of 30% is assigned to the vessel segment currents to allow variation in reconstruction. The fits typically match the estimates for the vessel currents to low tolerance. The poloidal flux contours for a plasma equilibrium reconstruction, as well as pressure and safety factor profiles and a comparison of the visible light image of the discharge are shown in Fig. 8. The reconstructed plasma vertical and radial position well matches the fast camera image, showing the plasma center shifted about 10 cm below the midplane. The induced current flowing in the vessel wall $I_{p-wall} = 70$ kA is on the order of plasma current: computed $I_p = 93$ kA and measured $I_{p-m} = 95$ kA at the time shown.

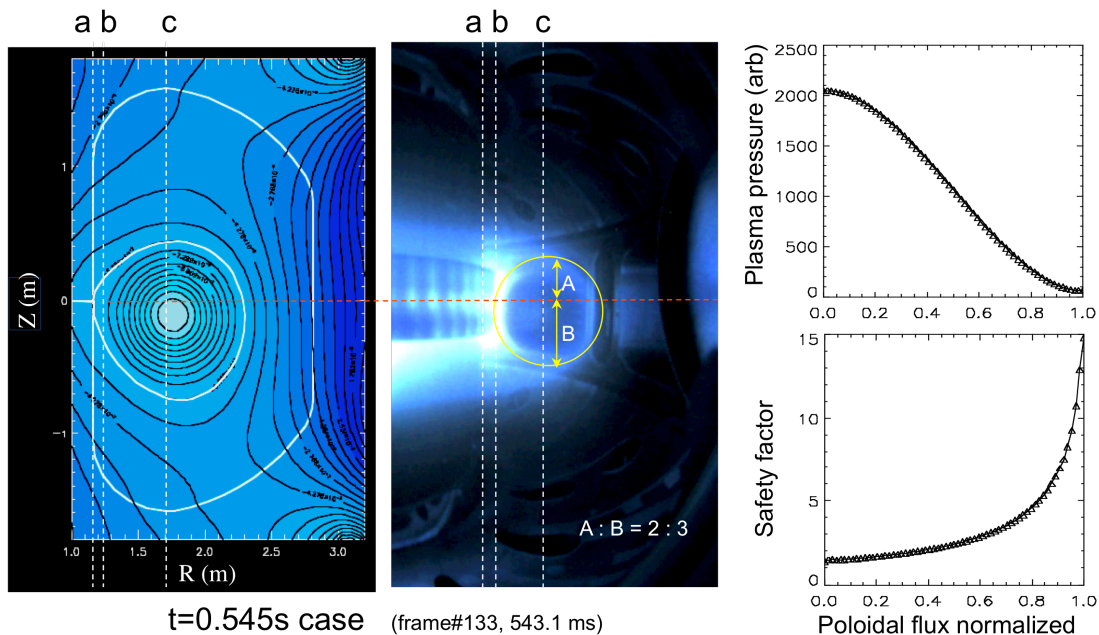


FIG. 8. Shot 1127 equilibria, fast camera data and profiles. a: $R=1.16$ m (vessel wall); b: $R=1.26$ m (inboard limiter); c: $R=1.7$ m (ECH pre-ionization resonance layer).

3. High Beta Operational Space and Ideal MHD Stability

Numerical analysis of envisioned high beta KSTAR plasmas based on the present machine design and experimental data from present tokamaks shows the potential of the device to demonstrate significant beta enhancement by stabilizing global MHD modes. Equilibria spanning the expected operational range of the device and constrained by coil system capabilities are computed using EFIT for various pressure and q profiles including generic L-mode and DIII-D experimental H-mode pressure profiles. The MHD stable operating space

for toroidal mode number, $n = 1$, modes as computed by the DCON stability code is shown in Fig. 9. RWM stabilization using a 3D representation of the KSTAR wall in VALEN is used to determine the best 2D representation of the device wall structure in DCON. The results show a wide range of l_i over which substantial improvements of β_N over $\beta_N^{no-wall}$ can be achieved in the device. For an H-mode pressure profile at plasma internal inductance, $l_i = 0.7$, passive MHD mode wall-stabilization allows operation at $\beta_N = 5$, which is a factor of two greater than for equilibria without passive stabilization, $\beta_N^{no-wall} = 2.5$. For the L-mode pressure profile, the wall-stabilized region is located at the lowest l_i . This is unfavorable for $n = 0$ stabilization, and therefore this operational space will likely be more restricted. As $n = 2$ RWMs were observed in NSTX [3], the KSTAR stable operating space for toroidal mode number $n = 2$ was also studied with the DCON stability code and results for H-mode and L-mode pressure profiles are shown in Fig. 10. $n = 2$ stability has higher no-wall and lower with-wall limits than $n = 1$.

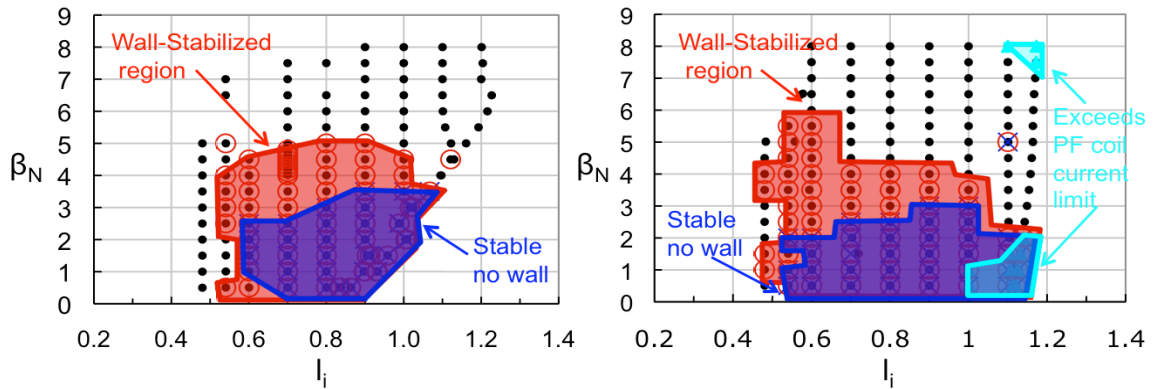


FIG. 9. Ideal MHD stability for $n = 1$ modes with H-mode (left) and L-mode (right) pressure profiles

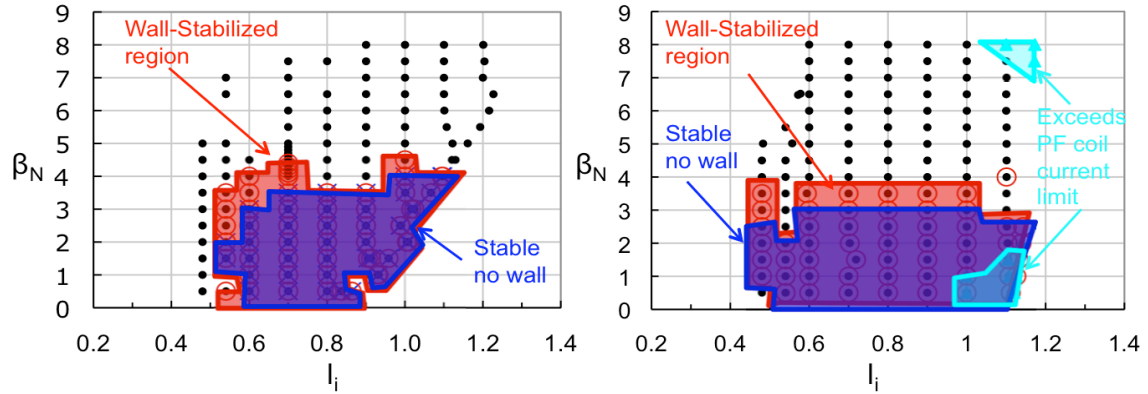


FIG. 10. Ideal MHD stability for $n = 2$ modes with H-mode (left) and L-mode (right) pressure profiles.

4. Resistive Wall Mode Stabilization at High β_N

KSTAR is designed to investigate active global MHD mode stabilization, which is required in plasmas with insufficient plasma rotation for passive stabilization, as expected in future burning plasmas including ITER [15]. Active control of RWMs has been investigated in present experimental devices including NSTX [5] and DIII-D [4] using classical feedback control with proportional gain. The stabilization system planned for KSTAR comprises passive stabilizing plates and actively cooled in-vessel control coils (IVCC), Fig. 11, designed for non-axisymmetric field error correction and stabilization of slow timescale MHD modes ($\gamma \sim 1/\tau_{wall}$) including the RWM. Fig. 12 illustrates the capability of active stabilization in KSTAR based on VALEN analysis using a classical control algorithm with standard proportional gain.

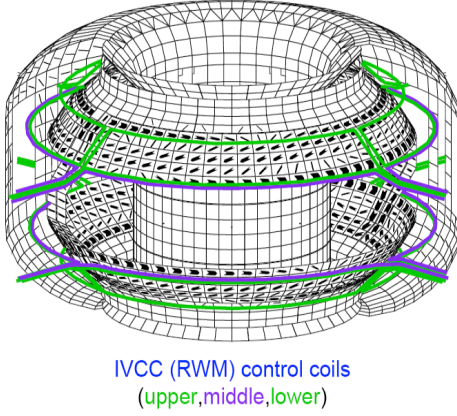


FIG. 11. Conducting hardware and IVCC set up in VALEN-3D based on engineering drawings

$L=10\text{mH}$; $R=0.86\text{m}\Omega$ with $L/R=12.8\text{ms}$ and fast IVCC circuit parameters were chosen to be $L=13\text{mH}$ $R=13.2\text{m}\Omega$ with $L/R=1.0\text{ms}$. The upper limit of the RMS power required to control RWM with fast IVCC is computed to be 62kW for $C_\beta = 80\%$ and 1.8MW for $C_\beta = 95\%$, $C_\beta \equiv (\beta_N - \beta_N^{\text{no-wall}})/(\beta_N^{\text{wall}} - \beta_N^{\text{no-wall}})$.

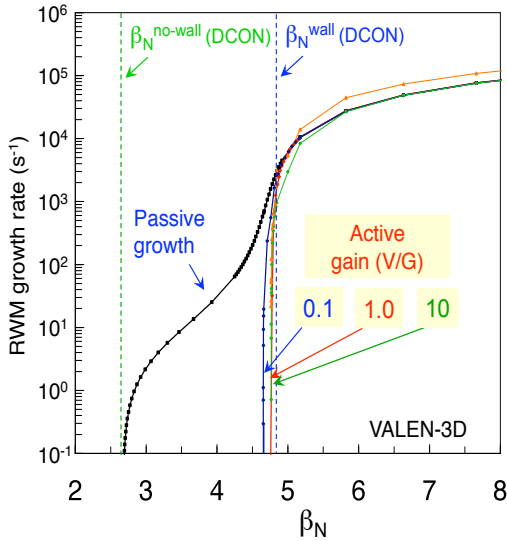


FIG. 12. VALEN computed growth rate for an $n = 1$ mode for passive and active feedback stabilization.

6. Conclusions

First plasma equilibria were reconstructed using EFIT including the vacuum vessel currents estimated by the VALEN code. Vacuum field shots give reasonable matches between measured and computed signals with relatively large error bars. The reconstructed plasma vertical and radial position well matches visible light from a fast framing camera. KSTAR is capable of producing long-pulse, high β_N stability research. The machine is designed to run high β_N plasmas with low l_i and significant plasma shaping capability. A large wall-stabilized region to kink/ballooning modes is computed with $\beta_N / \beta_N^{\text{no-wall}} = 2$ at the highest β_N predicted

The RWM structure was computed for the plasma equilibrium with $l_i = 0.7$ and $\beta_N^{\text{wall}} = 5$. The computed no-wall and with-wall β_N limits are in a good agreement with DCON analysis, represented by the vertical dashed line. Active stabilization near the ideal wall limit ($\beta_N = 4.76$) was reached with feedback gain $1.0\text{V/G} - 10\text{V/G}$ using the midplane segment of the IVCC.

RMS values of IVCC currents, voltages and power for the unloaded and fast IVCC circuit were calculated in the presence of white Gaussian noise, and noise based on NSTX active control experiments, as shown in Table 1. Unloaded IVCC circuit parameters were

5. Advanced state-space control algorithms for RWM Stabilization

Advanced state-space control algorithms are theoretically capable of reaching higher beta limits at reduced RMS system power than allowed by classical control techniques [16]. Present computations using an advanced Linear Quadratic Gaussian (LQG) controller, including balanced truncation of the VALEN state-space yield a factor of 2 power reduction assuming white noise for unloaded and fast IVCC as shown in Table 2. This performance is realized with the VALEN state-space reduced to as few as 3 states implementing balanced truncation techniques. A small state space makes the advanced control algorithm possible for real-time implementation. This controller is numerically proven to be robust with respect to variations in β_N .

for the device. The planned active IVCC mode control system provides RWM control, allowing active $n = 1$ RWM stabilization at very high $C_\beta > 98\%$. An IVCC circuit for stabilization is possible at reasonable power levels. Advanced controller techniques allow 50% power reduction compared to proportional gain controller.

TABLE 1: POWER ESTIMATES FOR RWM CONTROL WITH PROPORTIONAL GAIN

		White noise (1.6-2G RMS)			NSTX 120047 ΔB_p sensors		
<i>Unloaded IVCC</i> L/R=12.8ms	C_β	$I_{IVCC}(A)$	$V_{IVCC}(V)$	$P_{IVCC}(W)$	$I_{IVCC}(A)$	$V_{IVCC}(V)$	$P_{IVCC}(W)$
	80%	30	1.6	45	362	0.7	253
	95%	41	2.0	82	430	0.8	307
<i>Fast IVCC circuit</i> L/R=1.0ms	C_β	$I_{IVCC}(A)$	$V_{IVCC}(V)$	$P_{IVCC}(W)$	$I_{IVCC}(A)$	$V_{IVCC}(V)$	$P_{IVCC}(W)$
	80%	21	1.56	30.0	1.9e3	24.9	62e3
	95%	28.3	1.78	50.6	9e3	119	1.8e6

TABLE 2: RWM SYSTEM POWER REDUCTION USING ADVANCED LQG CONTROLLER

		White noise (1.6-2G RMS)		
<i>Unloaded IVCC</i> L/R=12.8ms	C_β	$I_{IVCC}(A)$	$V_{IVCC}(V)$	$P_{IVCC}(W)$
	80%	3%	50%	47%
	95%	15%	51%	58%
<i>Fast IVCC circuit</i> L/R=1.0ms	C_β	$I_{IVCC}(A)$	$V_{IVCC}(V)$	$P_{IVCC}(W)$
	80%	38%	75%	47%
	95%	15%	73%	58%

This research was supported by the U.S. Department of Energy under contract DEFG02-99ER54524.

-
- [1] M.C. Zarnstorff, et al. Phys. Rev. Lett. **60** (1988) 1306 .
[2] R.D. Stambaugh, V.S. Chan, R.L. Miller, et al., Fusion Technology **33** (1998) 1.
[3] S.A. Sabbagh, A.C. Sontag, J.M. Bialek, et al., Nucl. Fusion **46** (2006) 635.
[4] M. Okabayashi, et al., Phys. Plasmas **8** (2001) 2071.
[5] S.A. Sabbagh, R.E. Bell, J.E. Menard, et al., Phys. Rev. Lett., **97** (2006) 045004.
[6] E.J. Strait, et al., Phys. Plasmas **11** (2004) 2505 .
[7] A.J. Klein, D.A. Maurer, T.S. Pedersen, et al., Phys. Plasmas **12** (2005) 040703.
[8] G.S. Lee, J. Kim, S.M. Hwang, et al., Nucl. Fusion **40** (2000) 575 .
[9] G.S. Lee, J. Kim, S.M. Hwang, et al., Fusion Eng. Des. **46** (1999) 405.
[10] G.S. Lee, M. Kwon, C.J. Doh, et al., Nucl. Fusion **41** (2001) 1515.
[11] L.L. Lao, et al., Nucl. Fusion **25** (1985) 1611.
[12] J.M. Bialek, A.H. Boozer, M.E. Mauel, et al., Phys. Plasmas **8** (2001) 2170.
[13] S.A. Sabbagh, et al., Nucl. Fusion **41** (2001) 1601.
[14] S.G. Lee, J.G. Bak, E.M. Ka, J.H. Kim, and S.H. Hahn “Magnetic diagnostics for the first plasma operation in Korea Superconducting Tokamak Advanced Research”, to be published in Rev. Sci. Instrum. (October, 2008).
[15] Y. Liu, A. Bondeson, M.S. Chu, et al., Nucl. Fusion **45** (2005) 1131.
[16] O. Katsuro-Hopkins, J.M. Bialek, D.A. Maurer, et al., Nucl. Fusion **47** (2007) 1157.